antenna compared to the omnidirectional case. These results indicate improvements from reduced multipath and more Rician sector statistics, in agreement with [5].

Table 2: Performance comparisons

Name	Performance gain (Mode 4)	Performance gain (Mode 5)
	dB	dB
R1	7.3	5.5
R2	2.4	2.5
R3	1.5	1.3

Conclusions: Results with omnidirectional antennas at the MT and AP confirm that lower frequency selectivity reduces the coded performance of OFDM systems in Rayleigh fading. Channel R1 performs better than might be expected for such low RMS delay spreads since the channel exhibits a significant Rician characteristic.

Performance comparisons between omnidirectional and sectorised antennas clearly demonstrate that the average coded performance is significantly enhanced in all cases by sectorisation (Rayleigh or Rician, frequency selective or flat). In channels with a dominant multipath component, the correct choice of sector will reduce the multipath activity and improve the Rician statistics. As shown in Table 2, gains of up to 7.3dB occur. In channels with high angular spread and no dominant component, a small improvement will occur from six-sector antenna diversity.

The performance gains quoted in Table 2 are independent of the antenna gain (Table 1) offered by the sectorised antenna (antenna gain was normalised in the simulation). In cases where the sectorised antenna is used to receive (uplink), the antenna gain will offer an effective performance gain. This antenna gain is typically a few dB less than the 7.8dB theoretical maximum. The loss occurs owing to energy falling outside the main beam of the antenna (i.e. into other sectors). In a channel with low angular spread, the perceived antenna gain is close to the theoretical maximum, since the majority of received multipath falls in a single sector [4].

Clearly, despite reduced frequency selectivity, AP sectorisation offers a means of improving the performance of a HIPERLAN/2 link. In cases where the channel exhibits strong Rician characteristics, the gain can be extremely high, e.g. gains of 13.4dB on the uplink and 7.3dB on the downlink (with a further 7.8dB power saving) are possible for the mode 4 example considered in this Letter.

© IEE 2001

18 December 2000

Electronics Letters Online No: 20010165

DOI: 10.1049/el:20010165

A. Doufexi, S. Armour, A. Nix, P. Karlsson and D. Bull (*Centre for Communications Research, University of Bristol, Woodland Road, BS8 1UB, United Kingdom*)

E-mail: A.Doufexi@bristol.ac.uk

P. Karlsson: Also with Telia Research AB, Malmoe, Sweden

References

1 ETSI: 'Broadband radio access networks (BRAN); HIPERLAN type 2 technical specification; physical (PHY) layer', August 1999. ⟨DTS/BRAN-0023003⟩ V0.k

2 MEDBO, J., and SCHRAMM, P.: 'Channel models for HIPERLAN/2', ETSI/BRAN, 3ERI085B, 1998

3 DOUFEXI, A., ARMOUR, S., NIX, A., and BULL, D.: 'A comparison of HIPERLAN/2 and IEEE 802.11a physical and MAC layers'. IEEE Symp. Communications and Vehicular Technology, 2000, pp. 13–19

4 KARLSSON, P., BERGLJUNG, C., BORJESON, H., and PAMP, J.: 'Analysis and results of wideband spatial radio channel measurements at 5 GHz - Impact on multiple antenna systems'. AP2000, Davos, 9–14 April 2000

5 AWACS Final Report, CEC Deliverable No.: AWACS/CIT/PM1/DS/P/015/b1, September 1998

Performance of Rake receiver assisted adaptive-modulation based CDMA over frequency selective slow Rayleigh fading channels

B.J. Choi, M. Münster, L.-L. Yang and L. Hanzo

A closed form expression of the average bit error rate (BER) is derived for a Rake receiver based adaptive-modulation scheme over frequency selective slow Rayleigh fading channels. Multi-dimensional minimisation of a cost function based on the derived closed form BER expression is performed to optimise the switching levels for a constant BER adaptive modulation system.

Introduction: In adaptive quadrature amplitude modulation (AQAM) [1 – 3], the modulation mode is determined on a frame-by-frame basis depending on the near-instantaneous channel quality, in order to increase the throughput, while maintaining a given target BER. For the successful operation of adaptive modems, accurate channel quality estimation/prediction and switching level optimisation [4] are important. Assuming perfect channel quality estimation/prediction, here we focus on the analysis of the average BER of the Rake receiver assisted adaptive modem and on the optimisation of the switching levels. The performance of adaptive modems communicating over narrow-band Rayleigh channels [5] as well as over wide-band Rayleigh channels [6, 7] was reported before. However these results were based on simulations.

Average BER performance: The average BER $P_a(\bar{\gamma})$ of an adaptive modem using five modes (no transmission, BPSK, QPSK, 16-QAM and 64-QAM) is given as [5]

$$P_a(\bar{\gamma}) = P_r(\bar{\gamma};\{l_i\})/B(\bar{\gamma};\{l_i\}) \qquad (1)$$

where P_r is the BER of the AQAM scheme and B is the average throughput, both of which are dependent upon the average channel SNR $\bar{\gamma}$ and on the set of AQAM switching levels $\{l_i\}$.

The BER of the AQAM scheme $P_r(\bar{\gamma})$ is expressed as [5]

$$P_r(\bar{\gamma};\{l_i\}) = P_{r,BPSK}(\bar{\gamma},l_1,l_2) + 2P_{r,QPSK}(\bar{\gamma},l_2,l_3) + 4P_{r,16-QAM}(\bar{\gamma},l_3,l_4) + 6P_{r,64-QAM}(\bar{\gamma},l_4,\infty) \qquad (2)$$

For m-ary square QAM employing Gray mapping, the BER term $P_{r,m}$ in eqn. 2 can be written as [8]

$$P_{r,m}(\bar{\gamma};\alpha,\beta) = \int_{\alpha}^{\beta} \sum_i A_i Q(\sqrt{a_i\gamma})\, f(\gamma) d\gamma \qquad (3)$$

where A_i and a_i are constants, $Q(x)$ is the Gaussian Q-function defined as $Q(x) = [1/\sqrt{(2\pi)}]\int_x^{\infty} e^{-t^2/2}dt$ and $f(\gamma)$ is the PDF of the instantaneous SNR per symbol γ. The PDF $f(\gamma)$ for an ideal Rake receiver over multi-path Rayleigh fading channels is given as [9] (p. 802)

$$f(\gamma) = \sum_{k=1}^{L} \frac{\pi_k}{\bar{\gamma}_k} e^{-\gamma/\bar{\gamma}_k} \qquad (4)$$

where π_k is defined as $\pi_k \triangleq \prod_{i=1,i\neq k}^{L} \bar{\gamma}_k/(\bar{\gamma}_k - \bar{\gamma}_i)$ and $\bar{\gamma}_k$ is the average channel SNR of the kth multi-path component satisfying $\bar{\gamma} = \Sigma_{k=1}^{L} \bar{\gamma}_k$. Substituting $f(\gamma)$ of eqn. 4 into eqn. 3 and applying integration-by-part, the BER $P_{r,m}$ can be expressed as

$$P_{r,m}(\bar{\gamma};\alpha,\beta) = \sum_i \sum_{k=1}^{L} \Big[A_i\pi_k \Big\{ e^{-\alpha/\bar{\gamma}_k} Q(\sqrt{a_i\alpha}) - e^{-\beta/\bar{\gamma}_k} Q\Big(\sqrt{a_i\beta}\Big) \Big\} - \mu_k \Big\{ Q(\sqrt{a_i\alpha}/\mu_k) - Q\Big(\sqrt{a_i\beta}/\mu_k\Big) \Big\} \Big] \qquad (5)$$

where $\mu_k = \sqrt{[a_i\bar{\gamma}_k/(a_i\bar{\gamma}_k + 2)]}$.

On the other hand, the average AQAM throughput B is given as [5]

$$B(\bar{\gamma};\{l_i\}) = F(l_1,l_2) + 2F(l_2,l_3) + 4F(l_3,l_4) + 6F(l_4,\infty) \qquad (6)$$

where $F(\alpha, \beta) = \int_{\alpha}^{\beta} f(\gamma)d\gamma$. The average AQAM throughput B of eqn. 6 can be simplified to

$$B(\bar{\gamma};\{l_i\}) = F_c(l_1) + F_c(l_2) + 2F_c(l_3) + 2F_c(l_4) \qquad (7)$$

where the complementary cumulative distribution function (CDF) $F_c(l)$ can be calculated as

$$F_c(l) = \int_l^{\infty} f(\gamma) d\gamma = \sum_{k=1}^{L} \pi_k e^{-l/\bar{\gamma}_k} \quad (8)$$

Substituting $P_{r,m}$ of eqn. 5 and $F_c(l)$ of eqn. 8 into eqns. 2 and 7, respectively, the average BER $P_a(\bar{\gamma})$ of eqn. 1 can be expressed in a closed form.

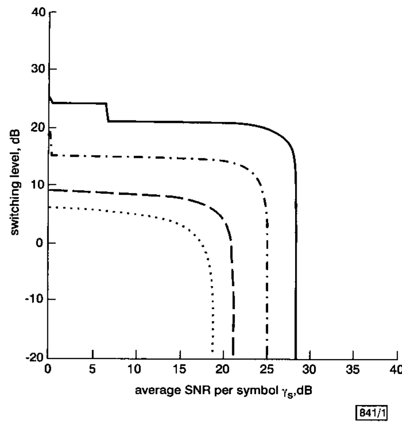

Fig. 1 *Optimised switching levels of five-mode AQAM system employing Rake receiver for target BER of $P_t = 10^{-3}$*

.... l_1
- - - - l_2
—·—·— l_3
——— l_4

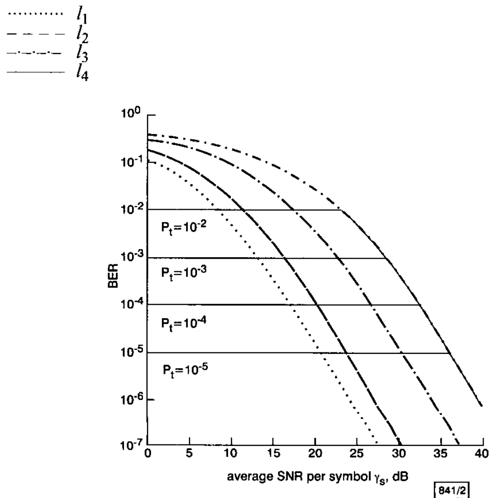

Fig. 2 *Average BER of Rake receiver assisted adaptive-modulation based CDMA*

P_t is target BER and dotted lines show BER of constituent fixed-mode schemes
.... BPSK
- - - - QPSK
——·—— 16-QAM
—· —· —· 64-QAM

Optimisation of AQAM switching levels: Torrance *et al.* [4] proposed the following cost function and applied Powell's optimisation for deriving the optimum switching levels:

$$\Omega(\{l_i\}) = \sum_{i=0}^{50} [10 \log_{10}(\max\{P_a(\bar{\gamma} = i\,\mathrm{dB}; \{l_i\})/P_t, 1\}) + B_t - B(\bar{\gamma} = i\,\mathrm{dB}; \{l_i\})] \quad (9)$$

where P_t is the target BER and B_t is the target BPS of 6, which is the throughput of the highest modulation mode, namely 64-QAM in our scenario. Eqn. 9 allows us to produce a set of switching levels $\{l_i\}$, which is fixed for the whole SNR range. However, the corresponding average BER is not constant, implying that the average throughput can be potentially further increased, whilst still meeting the target BER. We propose a modified cost function $\Lambda(\bar{\gamma}; \{l_i\})$, putting more emphasis on achieving a higher throughput and aim for optimising the switching levels for a given SNR rather than for the whole SNR range. This cost function is formulated as

$$\Lambda(\bar{\gamma}; \{l_i\}) = 10 \log_{10}(\max\{P_a(\bar{\gamma}; \{l_i\})/P_t, 1\}) + \rho \log_{10}(B_t / B(\bar{\gamma}; \{l_i\})) \quad (10)$$

where ρ is a weighting factor, allowing us to aim for a BPS throughput enhancement. Applying Powell's optimisation [10] using this cost function under the constraint of $0 \le l_1 \le l_2 \le l_3 \le l_4$, the optimum switching level set $\{l_i\}_{\bar{\gamma},opt}$ can be obtained.

Table 1: Average SNR in dB required for achieving target BER of 10^{-3}

BPS	SNR, dB		
	Fixed	Adaptive	Gain
1	13.187	8.152	5.035
2	16.197	12.334	3.863
4	22.659	19.112	3.547
6	28.418	28.418	—

Results and conclusion: As an example, we use a 3-path fading channel model derived from an indoor wireless asynchronous transfer mode (WATM) environment [8], where the average SNR for each path is given as $\bar{\gamma}_1 = 0.79192\bar{\gamma}$, $\bar{\gamma}_2 = 0.12424\bar{\gamma}$ and $\bar{\gamma}_3 = 0.08384\bar{\gamma}$. The optimised switching levels are depicted in Fig. 1, where the target BER P_t was 10^{-3} and the weighting factor in eqn. 10 was ρ = 3. Fig. 1 suggests that the lower-order modulation modes are abandoned one by one as the average SNR increases, in order to increase the average throughput. For example, the BPSK mode is unlikely to be invoked by the AQAM modem, when the average channel SNR is in excess of 19dB, and hence l_1 rapidly approaches zero or $-\infty$ in dB, as shown in Fig. 1. The average BER of our AQAM system depicted in Fig. 2 shows that the modem maintains the required constant target BER, until it reaches the BER curve of the fixed-mode modulation scheme employing the highest-order modulation mode, and then it drops. Table 1 summarises the SNR gain of the AQAM schemes over the constituent fixed modulation schemes for the target BER of 10^{-3}. For the average throughput of 1 BPS, the fixed BPSK modem required an average channel SNR of 13.187dB, whereas the AQAM scheme required 8.152dB, exhibiting over 5dB SNR gain. However, this SNR gain was decreased in comparison to higher throughput fixed schemes. In terms of the average throughput, the AQAM scheme provided more than 1 BPS throughput gain over the fixed schemes for a given SNR. This additional throughput can be invested into channel coding for ensuring that the system exhibits virtually error-free performance.

In conclusion, we found that Rake receiver assisted AQAM can be configured as a fixed BER system, while providing a variable throughput as a function of the average channel SNR. The adaptive arrangement was shown to outperform the conventional fixed-throughput/variable-BER system. Since we assumed perfect channel SNR estimation/prediction, the observed performance gain constitutes the upper-bound performance.

© IEE 2001
12 December 2000
Electronics Letters Online No: 20010176
DOI: 10.1049/el:20010176

B.J. Choi, M. Münster, L.-L. Yang and L. Hanzo (*Department of Electronics and Computer Science, University of Southampton, Southampton SO17 1BJ, United Kingdom*)

E-mail: lh@ecs.soton.ac.uk

References

1 WEBB, W., and STEELE, R.: 'Variable rate QAM for mobile radio', *IEEE Trans. Commun.*, 1995, **43**, pp. 2223–2230

2 GOLDSMITH, A.J., and CHUA, S.G.: 'Variable rate variable power MQAM for fading channels', *IEEE Trans. Commun.*, 1997, **45**, pp. 1218–1230

3 SAMPEI, S., KOMAKI, S., and MORINAGA, N.: 'Adaptive modulation/TDMA scheme for large capacity personal multimedia communications systems', *IEICE Trans. Commun.*, 1994, **E77-B**, pp. 1096–1103

4 TORRANCE, J.M., and HANZO, L.: 'Optimization of switching levels for adaptive modulation in slow Rayleigh fading', *Electron. Lett.*, 1996, **32**, pp. 1167–1169

5 TORRANCE, J.M., and HANZO, L.: 'On the upper bound performance of adaptive QAM in a slow Rayleigh fading', *Electron. Lett.*, 1996, **32**, pp. 169–171

6 WONG, C.H., and HANZO, L.: 'Upper-bound performance of a wideband burst-by-burst adaptive modem'. Proc. 49th IEEE Vehicular Technology Conf., Amsterdam, September 1999, Vol. 3, pp. 1851–1855

7 KUAN, E.L., and HANZO, L.: 'Burst-by-burst adaptive joint detection CDMA'. Proc. 49th Vehicular Technology Conf., Amsterdam, September 1999, Vol. 2, pp. 1628–1632

8 WEBB, W.T., HANZO, L., and KELLER, T.: 'Single- and multicarrier modulation; principles and applications for personal communications, WLANs and broadcasting' (IEEE Press and John Wiley & Sons, 2000)

9 PROAKIS, J.G.: 'Digital communications' (McGraw Hill International Editions, 1995), 3rd edn.

10 PRESS, W.H., FLANNERY, B.P., TEUKOLSKY, S.A., and VETTERLING, W.T.: 'Numerical recipes in C' (Cambridge University Press, 1992)

GaN/SiC *p-n* mesa junctions for HBTs fabricated using selective photoelectrochemical etching

J.W. Graff, E.F. Schubert and A. Osinsky

GaN/SiC *p-n* junctions for heterojunction bipolar transistors have been fabricated using photoelectrochemical etching. The process was shown to have excellent selectivity between *n*- and *p*-type semiconductors, self-terminating at the *p*-type SiC layer. Smooth *p*-SiC surfaces were observed, and contact resistance on the etched surface of $3 \times 10^{-3}\Omega cm^2$ was achieved. This process has been used in the fabrication of HBTs.

Introduction: The wide bandgap semiconductors GaN and SiC have emerged as important materials for high performance electronic and optoelectronic devices. Recently, high electron mobility transistors (HEMTs) based on AlGaN/GaN heterostructures [1], as well as high performance SiC metal semiconductor field effect transistors (MESFETs) [2], have been demonstrated. However, bipolar devices, including heterojunction bipolar transistors (HBTs), are also of great interest owing to the better linearity and greater power density attainable.

A number of obstacles exist in producing high performance HBTs based on GaN and SiC heterostructures. For the AlGaN/GaN system, the inherently high resistivity of *p*-GaN currently limits device performance. Alternatively, the growth of a wide bandgap GaN emitter on conductive *p*-SiC base can avoid this problem, provided high quality emitter-base heterojunctions can be attained. From a processing standpoint, the low etch selectivity between emitter and base during plasma etching, as well as degradation of base contact resistance, are obstacles to devices based on using either material [3]. In this Letter we demonstrate a novel method of relieving both of these problems, based on a highly selective, low damage wet chemical etch.

Experiment: The *p-n* junctions examined in this study are formed by the GaN emitter and SiC base layers of an HBT wafer. The structures were epitaxially grown on conductive *n*-type 4H SiC substrates. A 0.7μm *n*-type SiC collector was grown by standard chemical vapour deposition, followed by a 0.2μm *p*-type SiC base layer. Following the SiC epitaxy, a 0.25μm-thick *n*-type GaN emitter was grown using the hydride vapour phase epitaxy (HVPE) technique.

Device processing for *p-n* junctions began with the e-beam deposition of a Ti/Al/Ni/Au ohmic contact to the *n*-GaN emitter. This metal also served as a mask for the etch process. Emitter mesa definition was performed using photoelectrochemical (PEC) etching. In this method, the sample is placed in a dilute aqueous solution of KOH (~0.04M) and exposed to ultraviolet light from a mercury arc lamp (at an intensity of ~10mW/cm²). A 1.0V bias was applied between the semiconductor and the etch solution during the process. After formation of the emitter mesa, Al/Ti/Au contacts to the *p*-SiC base were formed. Finally, the structures were annealed for 30s at 800°C in a nitrogen ambient to reduce contact resistance.

Results and discussion: Photoelectrochemical (PEC) etching has been shown to be selective to conductivity type in both GaAs and GaN materials [4, 5]. This method employs above bandgap radiation to generate electron-hole pairs inside the semiconductor. Assuming a pinned surface potential, an electric field exists which forces photo-generated holes to the surface in an *n*-type semiconductor and drives holes towards the bulk in a *p*-type semiconductor. The excess of holes at the surface in the *n*-type case makes the material susceptible to chemical attack. Conversely, the excess of electrons at the surface of a *p*-type semiconductor effectively strengthens chemical bonds, further resisting dissociation.

During the PEC etch process, the current between two neighbouring emitter contacts was monitored as a function of etch time. This result is shown in Fig. 1. The current decreases by more than three orders of magnitude after 25min of etching. No further change in current is observed for longer etch times, indicating that this residual current may be due to leakage through the base-emitter junction. This also implies that all of the GaN layer has been etched away.

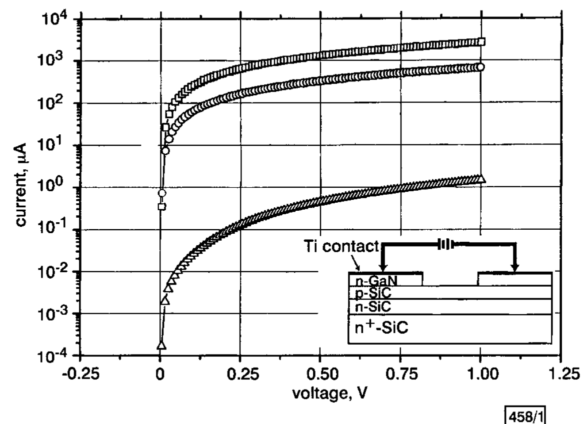

Fig. 1 *Measured I-V characteristics between two n-type contacts*

Significant reduction in current implies complete removal of *n*-type layer
□ 5min
○ 10min
△ 25min

The etch profile of the resulting emitter mesa measured with a contact profilometer is shown in Fig. 2. Two points are evident from the Figure. First, the significant GaN surface roughness. We attribute this roughness to the use of off-axis 4H SiC substrates, which are more suitable for SiC epitaxy but less so for GaN growth. The second feature of note is the very smooth exposed *p*-SiC surface. This surface was measured to have an RMS roughness < 50Å, which is less than the resolution of the profilometer.

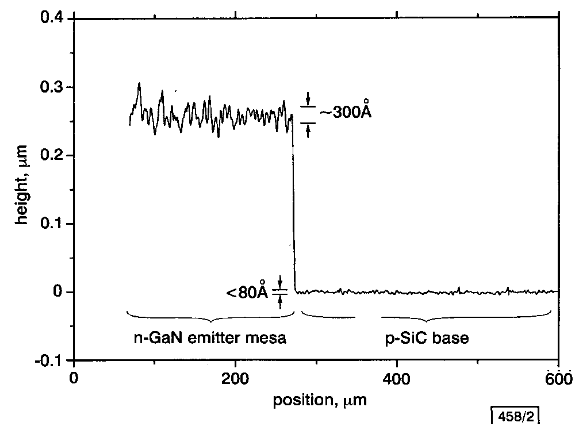

Fig. 2 *Etch profile of n-GaN/p-SiC mesa diode*

The I-V characteristic of the *p-n* junction diode is shown in Fig. 3. The diode characteristic appears quite resistive, owing to the small thickness of the base and the relatively low conductivity